Journal of Natural Gas Science and Engineering 21 (2014) 304–315

Contents lists available at ScienceDirect

Journal of Natural Gas Science and Engineering

journal homepage: www.elsevier.com/locate/jngse

Control technique on navigating path of intersection between two horizontal wells

Baobin Xi*, Deli Gao

State Key Laboratory of Petroleum Resource and Prospecting, College of Petroleum Engineering, China University of Petroleum-Beijing, Beijing 102249, China

ARTICLE INFO

Article history:
Received 15 July 2014
Received in revised form
20 August 2014
Accepted 21 August 2014
Available online

Keywords:
U-shaped well
Horizontal well
Intersection
RMRS
Profile design: trajectory control
Uncertainty analysis

ABSTRACT

The intersection between two horizontal wells is a form of U-shape well. Being efficient, economical, advanced and environmentally friendly, it holds broad application prospects in exploitation of resources and crossing of pipe lines and tunnels under rivers. However, it is very difficult to achieve intersection between two horizontal wells by conventional techniques due to borehole position uncertainty. In order to solve this problem, control technique on navigating path was put forward. It mainly consists of position locating technique, profile design method, trajectory control method and relative position error analysis. Firstly, the measurement of relative position between the bit and the intersection point was carried out by RMRS in closed-loop mode rather than traditional open-loop mode. Then the profile of the intersection between two horizontal wells was designed according to the ranging scope of RMRS, guide process and borehole position uncertainty. After that the trajectory control model in the intersecting process was established on the basis of an analogy between the intersection of the two horizontal wells and the plane landing process. Finally, the relative position error analysis was carried out according to the guide process of RMRS. The development of control technique on navigating path make it more feasible to achieve intersection between two horizontal wells, which will have a great reference value for in-depth study and field application in the future.

1. Introduction

U-shaped wells technology means to connect two or more wells, which are hundreds of meters away from each other on the ground, hundreds or even thousands of meters underground using directional drilling and horizontal drilling technology (Gao et al., 2011). It is mainly used in exploitation of salt mineral (Peng et al., 2009), heavy oil (Poloni et al., 2010; Nie et al., 2012; Ibatullin et al., 2009), coal-bed methane (Cunnington and Hedger, 2010; Shen et al., 2012; Zhang et al., 2013), alkaline mineral, underground gasification mining of coal bed (Liu et al., 2005) and crossing of pipe lines and tunnels under rivers etc. It has been proved by practices that: the application of U-shaped wells technology can increase the production rate, recovery ratio and decrease the cost; U-shaped wells technology works better than others in extracting heavy oil; U-shaped wells technology is an important potential access to develop gas hydrate; U-shaped wells technology or similar technologies must be used to cross pipe lines and tunnels under rivers (Mullin et al., 2013; Li and Dai, 2008).

The U-shaped wells can be divided into three types according to types of the two wells connected: intersection between a horizontal well and a vertical well, intersection between a horizontal well and a directional well and intersection between two horizontal wells. The object of this study is the last one. In order to solve the problem of low intersection accuracy between two horizontal wells, control technique on navigating path of intersection between two horizontal wells is put forward as follows: a technique confirming the relative position between two wells by collecting information from a target well in an intersection well or in the other way around to guide an intersection well to joint with a target well accurately. This technique mainly consists of position locating technique, profile design method, trajectory control method and relative position error analysis.

A detailed theoretical analysis about the main content of control technique on navigating path of intersection between two horizontal wells and corresponding examples will be given in this article.

2. Position locating technique

Measuring tools are essential to achieving accurate connection of two wells underground. As a traditional measurement tool,

* Corresponding author. Tel.: +86 18810524500.
E-mail address: 2011312010@student.cup.edu.cn (B. Xi).

http://dx.doi.org/10.1016/j.jngse.2014.08.020
1875-5100/

MWD cannot meet this demand due to the measurement accuracy and its lag, uncertainty of target connection and calculation error of trajectory measurement (Lee and Brandao, 2005). Therefore, the magnetic ranging tool is introduced to achieve a connection mechanically and hydraulically between two wells in the final stage. Rotating magnetic ranging system (RMRS) is chosen to measure the relative position after an analysis of existing commercial magnetic ranging tools (Kuckes et al., 1996; Oskarsen et al., 2009; Al-Khodhori et al., 2008).

2.1. Working principle

RMRS mainly consists of a magnetic sub, a probe and a ranging software. It is able to detect the distance between two adjacent wells while drilling and control the trajectory of complex-structure wells accurately. RMRS for Intersection between two horizontal wells is shown in Fig. 1. The magnetic sub near the bit is a short non-magnetic drill collar embedded with several permanent magnets perpendicularly. It rotates with the drill string to generate the alternating magnetic field which serves as magnetic source of RMRS. The probe consists of a sensor package composed of a tri-axial fluxgate sensor and a tri-axial accelerometer sensor. It is used to detect the direction it points in the wellbore and the induction density of alternating magnetic field generated by rotating magnetic sub (Diao et al., 2012). After calculating the relative position with ranging software based on the magnetic signal data, the horizontal wells can be accurately connected by continuously adjusting the trajectory.

2.2. Calculation of the relative position

As shown in Fig. 2, three coordinate systems are established. *O–NED* is a geodetic coordinate system, where *O* is the origin, *N* points north, *E* points east and *D* points to the geocenter. Taking *p*, the center point of magnetic sub which can be regarded as the current bottom hole, as the origin, the right-hand Cartesian coordinate system *p-xyz* can be established at the bottom hole, where *z* points to the drilling direction, *x* points to the high-side direction of the wellbore and *y* is determined by the right-hand rule. Taking *t*, the intersection point, as the origin, the right-hand Cartesian coordinate system *t-XYZ* can be established, where *Z* points to the extension direction of the horizontal well, *X* points to the high-side direction of the wellbore and *Y* is determined by the right-hand rule.

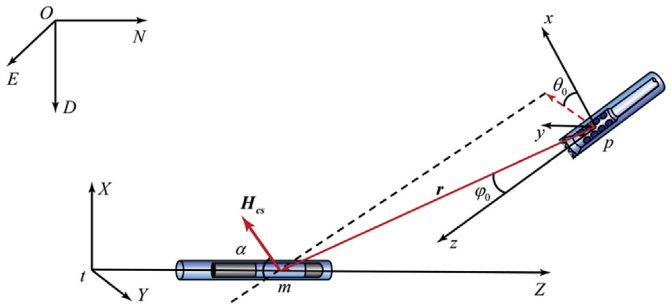

Fig. 2. Establishment of coordinate systems.

$m(r,\theta_0,\varphi_0)$, the center point of probe, measured by RMRS is the position of the measure point *m* in the local coordinate system *p-xyz*, where *r* is the relative distance, *m*; θ_0 is the relative tool face, (°); and φ_0 is the relative azimuth, (°).

α is the angle between $\mathbf{H}_{cs}$ and *z*-axis, then:

$$\tan\alpha = \frac{\sqrt{H_{csx}^2 + H_{csy}^2}}{H_{csz}} = \frac{3\sin 2\varphi_0}{3\cos 2\varphi_0 - 1} \tag{1}$$

where $\mathbf{H_{csx}}$, $\mathbf{H_{csy}}$ and $\mathbf{H_{csz}}$ represent components of the reference field $\mathbf{H}_{cs}$ in *x*, *y* and *z*-axis respectively.

$$\tan\theta_0 = \frac{H_{csy}}{H_{csx}} \tag{2}$$

The magnetic field at any point $m(r,\theta_0,\varphi_0)$ is elliptically polarized due to the dynamic rotation. The relationship between the minimum magnetic field strength and the distance *r* is expressed as follows:

$$r = \sqrt[3]{M/4\pi H_{min}} \tag{3}$$

The relative distance *r*, relative azimuth φ_0 and relative tool face θ_0 between any point and the origin in the rotating magnetic dipole coordinate system can be determined by Eqs. (1)–(3).

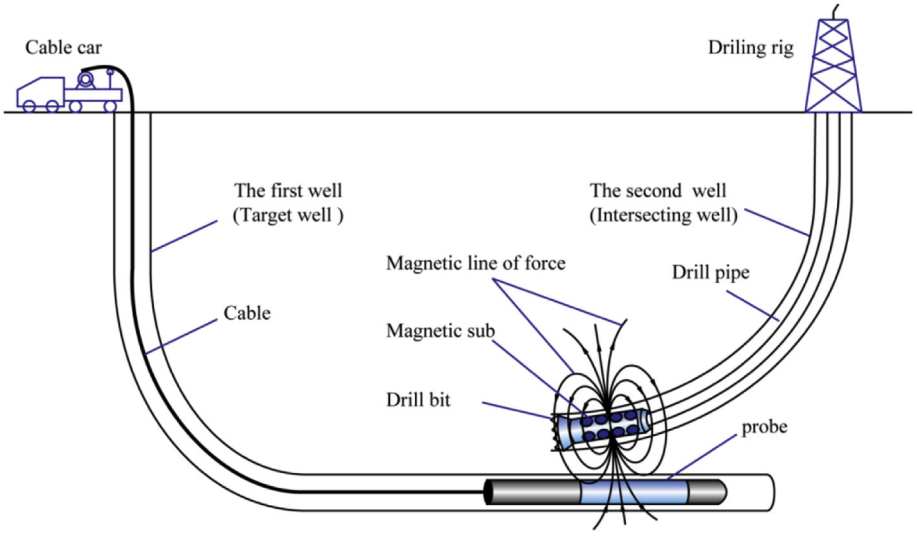

Fig. 1. Operational view of RMRS for Intersection between two horizontal wells.

3. Profile design method

The profile of intersection between two horizontal wells is designed with consideration of ranging scope limitations of RMRS, conditionality in guide process and trajectory uncertainty. As shown in Fig. 3, both horizontal wells are designed to be double build-up profiles in the same vertical plane. The two horizontal wells are accurately interconnected at point t.

"Line O_1a_1 – arc a_1b_1 – line b_1c_1 – arc c_1t_1 – line t_1d_1", which was drilled firstly, is called target well. R_1 and R_2 are radiuses of the two arcs, m; D_{t1} is the true vertical depth of the target, m; S_{t1} is the closure distance of the target, m. Horizontal segment e_2d_1 is named extension segment with its length denoted as S_{ext}, m. Horizontal segment e_1e_2 is named to-be-intersected segment with its length denoted as S_{int}, m, and the intersection point is in the to-be-intersected segment. In the ideal case, the intersection point t coincides with point e_2.

"Line O_2a_2 – arc a_2b_2 – line b_2c_2 – arc c_2t_2 – line t_2d_2", which was drilled later, is called intersecting well. R_3 and R_4 are radiuses of the two arcs, m; D_{t1} is the true vertical depth of the target, m; S_{t1} is the closure distance of the target, m.

"Arc d_2d_3 – arc d_3t – line td_4" is the transitional segment between two horizontal wells. Further on, "arc d_2d_3 – arc d_3t" which appears as S-shaped profile is called intersection segment. In this segment, the two arcs are of the same radius, denoted as R, m, which is a constant in the design. The lengths of the two arcs are denoted as Δl_1 and Δl_2, m; horizontal section td_4 is called overlap segment with its length denoted as S_{oli}, m.

Next, the design objective, influence factor and calculation equation about the key section will be given, which includes intersection segment, extension segment, to-be-intersected segment and overlap segment.

3.1. Intersection segment

The profile of the intersection segment is S-shaped, which is aimed at eliminating the horizontal offset S_d and vertical offset D_d between bottoms of the two horizontal wells, so as to achieve a smooth transition between two wells.

Three factors are taken into consideration in the design process of vertical offset D_d as follows:

(1) Improve the success rate of intersection. The intersection belongs to "point to point" without the vertical offset; otherwise, it belongs to "point to line", which is obviously much easier to achieve. In the second scenario, the intersecting process between the two wells is analogous to the plane landing process: the bit is like a plane, while the horizontal section of the target well is like a runway. Simply increase the inclination and the vertical depth of the intersecting well to achieve the intersection through the "landing type", which relies on gravity (Jia and Wang, 2004).

(2) Maximize effectiveness of the magnetic ranging tool. The magnetic ranging tools generate a constant magnetic field which can be more effectively measured in particular orientations at particular locations around it. These locations or orientations may be referred to as "sweet spots" of the ranging tool. As shown in Fig. 4, the shaded area is the "sweet spots" (Lee and Brandao, 2005; Kuckes et al., 1996). It can be seen that a vertical offset will help to locate the sensor within or near the "sweet spots", ending up with measurements closest to the real value.

(3) Minimize the effect of positional uncertainty on the intersection process. A vertical offset large enough ensures that the intersecting well is on the known side of the target well regardless of the positional uncertainty. This will provide a known direction to steer towards so as to close the gap between the boreholes even if the distance between the boreholes initially outranges the RMRS.

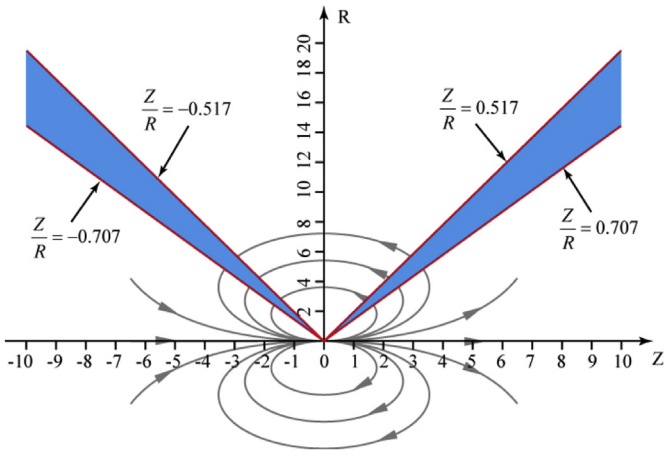

Fig. 4. The "sweet spots".

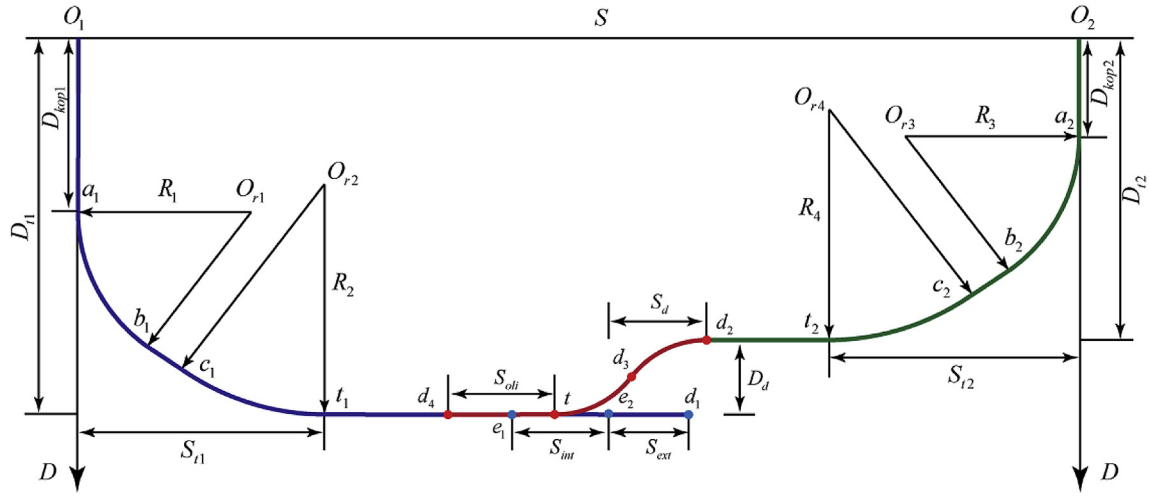

Fig. 3. Profile design.

The vertical offset D_d is determined by ranging scope of the RMRS and borehole position uncertainty both at d_2 on the intersecting well and e_2 on the target well.

So the range of D_d is:

$$r_{com} < D_d < r_m - r_{com} \tag{4}$$

where r_m is the ranging scope of RMRS, m; r_{com} is the length of the semi-major axis of the error ellipse determined by the borehole position uncertainty at d_2 combined with that at e_2, m.

The horizontal offset S_d is determined by D_d:

$$S_d = 2\sqrt{RD_d - D_d^2/4} \tag{5}$$

It is easy to get the lengths of the arcs in the intersection segment:

$$\Delta l_1 = \Delta l_2 = \frac{R\pi \arccos \frac{R - D_d/2}{R}}{180} \tag{6}$$

3.2. Extension segment

The distance between d_2 and e_2 may outrange RMRS due to its short ranging scope, in which case an extension segment could help to make better use of RMRS in the intersecting process, ending up with accurate intersection between the two horizontal wells. As shown in Fig. 5, in the guide process of RMRS, n and n′ is a pair of measure points: n is the position of the probe and n′ is the position of the magnetic sub.

It can be seen from Fig. 5 that the length of the extension segment is determined by three factors: vertical offset, ranging scope of RMRS and borehole position uncertainty both at d_2 on the intersecting well and e_2 on the target well.

The calculation formula for the extension segment is:

$$S_{ext} = S_d - \sqrt{r_m^2 - (D_d + r_{com})^2} \tag{7}$$

3.3. To-be-intersected segment

Given the borehole position uncertainty and a fixed radius of curvature R of the intersection segment, the intersection position can only be aimed at a segment e_1e_2 rather than a certain point on the target well. This segment is designed to eliminate the influence of borehole position uncertainty on the intersection process and facilitate preparatory work for the intersection such as running the glass casing and reaming.

It can be seen from Fig. 6 that the length of the to-be-intersected segment is determined by three factors: vertical offset, radius of curvature R in the intersection segment and borehole position uncertainty both at d_2 on the intersecting well and e_2 on the target well.

The calculation formula for the intersection segment is:

$$S_{int} = 2\sqrt{R\left(D_d + r_{com}\right) - (D_d + r_{com})^2/4} - S_d \tag{8}$$

3.4. Overlap segment

The overlap segment refers to the distance the bottom hole assembly (BHA) goes through in the target well after the intersection. This segment is designed to ensure the BHA goes into the target well without sidetracking, so as to establish a smooth borehole. There is no specific limitation length of overlap segment, as long as it fulfills the design purpose.

3.5. Case study

Given: in a profile design of intersection between two horizontal wells, the build-up rate of the intersection segment is 8°/30 m; r_{com} = 10 m; RMRS is selected as the magnetic ranging tool, and r_m = 70 m; according to Eq. (4), the vertical offset design value is D_d = 20 m.

Then how to reasonably design each segment?

From the equations: horizontal offset is S_d = 129.57 m; the length of intersection segment is $\Delta l_1 = \Delta l_2$ = 131.62 m; extension segment is S_{ext} = 66.33 m; to-be-intersected segment is S_{int} = 28.17 m.

For ease of analysis, the trends of some segment lengths relative to the influencing factors were graphed.

As shown in Fig. 7, the length of horizontal offset, extension segment and to-be-intersected segment tend to decrease along with the increase of the build-up rate. When the build-up rate is less than 1°/30 m, the lengths vary rapidly; when the build-up rate is greater than 3°/30 m, the lengths tend to level off. Therefore, a larger build-up rate is recommended for the intersection segment. In this case, a small deviation of the actual build-up rate from the designed one caused by formation and drilling parameters will not result in great change in the length of horizontal offset, extension segment and to-be-intersected segment, which improves fault tolerance of the design.

As shown in Fig. 8, with the increase in vertical offset, the length of horizontal offset and extension segment increase largely while the length of to-be-intersected segment tends to decrease gently. Therefore, a reasonable value of the vertical offset is required, or it can result in longer extension when too large and longer to-be-intersected segment when too small, both of which cause increase in cost of drilling.

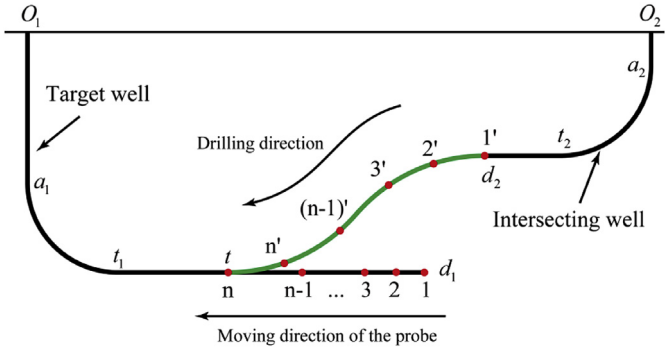

Fig. 5. The guide process of RMRS.

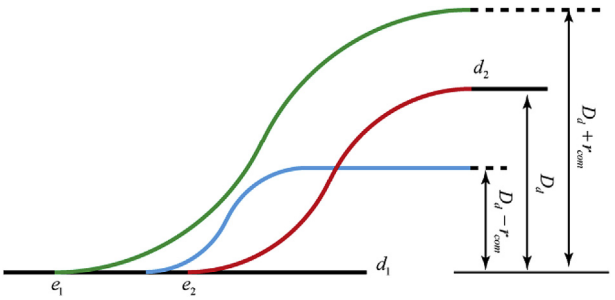

Fig. 6. The effect of uncertainty on segment to be connected.

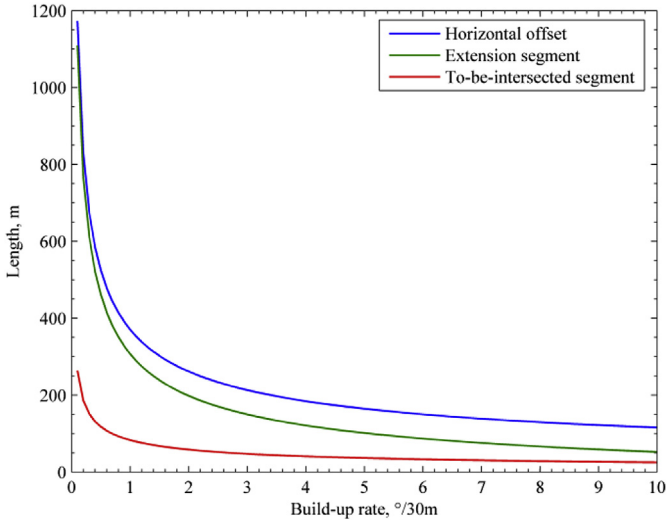

Fig. 7. The influence of build-up rate.

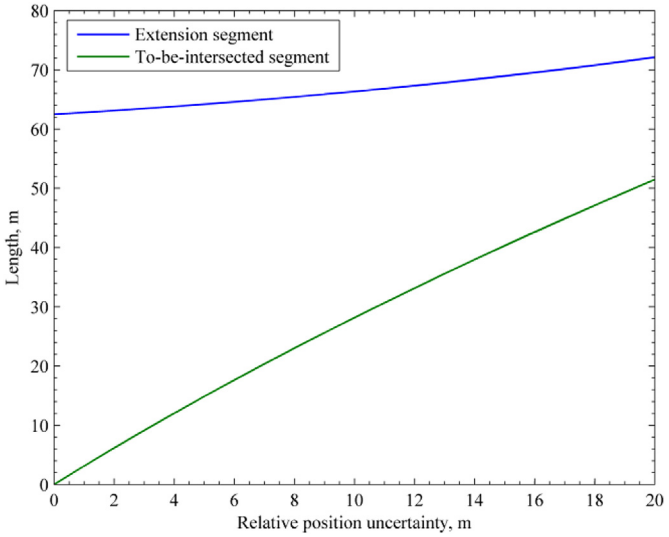

Fig. 9. The influence of uncertainty.

As shown in Fig. 9, with the increase of borehole position uncertainty, the length of to-be-intersected segment increases significantly, while the length of extension segment increases relatively gently. It can be seen that the borehole position uncertainty is an unfavorable factor for each segment. Therefore, the borehole position uncertainty must be theoretically assessed accurately using uncertainty model, and it sets a standard for error control in drilling, so as to finish the intersection between two horizontal wells successfully.

4. Trajectory control method

Higher requirements on the borehole trajectory design and control are put forward in order to achieve accurate intersection between two horizontal wells. Studies and discussions on trajectory design with a given direction at target have been on among many scholars. However, the existing methods are not suitable for the intersection between two horizontal wells as the point measured by RMRS is just a general measure point rather than the target.

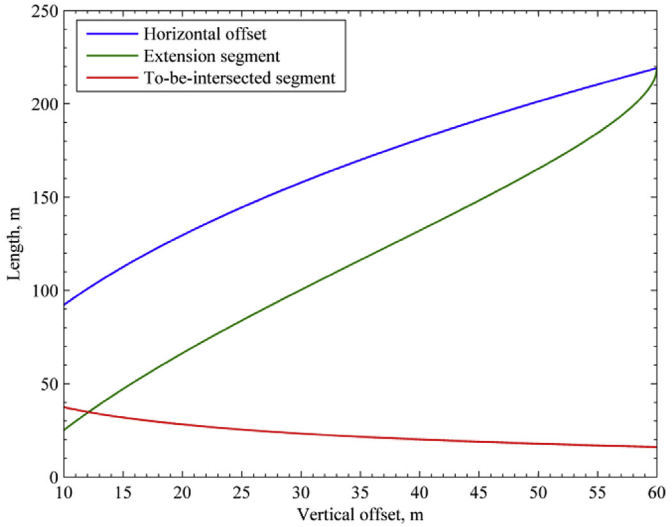

Fig. 8. The influence of vertical offset.

The main parameter for trajectory control in the intersecting process is azimuth, which, if deviates beyond the allowable range from required azimuth calculated by RMRS, needs to be brought back appropriately. The ending point of the adjusting segment is also crucial while controlling the direction. Dean Lee made an analogy between the intersection between two horizontal wells and the plane landing process in case study of the world's first U-shaped wells (Lee and Brandao, 2005). Liu Xiushan proposed the soft landing model, which was based on similarity between horizontal well landing and plane landing (Liu and He, 2002). In this analogy, the bit is compared to a plane, while the to-be-intersected segment of the target well is compared to a runway. In order to make an accurate and smooth drilling into the to-be-intersected segment, it is necessary to ensure trajectory of the intersecting well in the same vertical plane with to-be-intersected segment during the intersection. And then the intersection will be finished through the "landing style". From the foregoing, ending point of the adjusting segment must be in the vertical plane determined by the to-be-intersected segment, so that the intersection would be finished only by increasing inclination and vertical depth in the next step.

Trajectory control model for intersecting process between two horizontal wells would be established by using hold-inclination-and-adjust-azimuth pattern.

4.1. Establishment of control model

As shown in Fig. 10, *O–NED* is a geodetic coordinate system, and *p–xyz* is a coordinate system at the bottom of the intersecting well. The point *m* is a measure point at the target well. The vertical plane determined by the to-be-intersected segment is denoted by *V* with **n** being its unit normal vector. Horizontal plane H and vertical plane *V* intersect at AB.

The profile from *p* to *d* consists of four segments, "line *pa* — arc *ab* — arc *bc* — arc *cd*", the lengths of which are ΔL_1, ΔL_2, ΔL_3 and ΔL_4, *m*, respectively. The three arcs are finished by using hold-inclination-and-adjust-azimuth pattern and their tangent lengths are u_1, u_2 and u_3, *m*, respectively. The vertical plane determined by the borehole tangent at point *b* parallels *V*. The perpendicular distance from *c* to *V* is half the perpendicular distance from *b* to *V*. In addition, the horizontal projection of the profile on the plane H is "straight line $p'a'$ — curve $a'b'$ — curve $b'c'$ — curve $c'd'$".

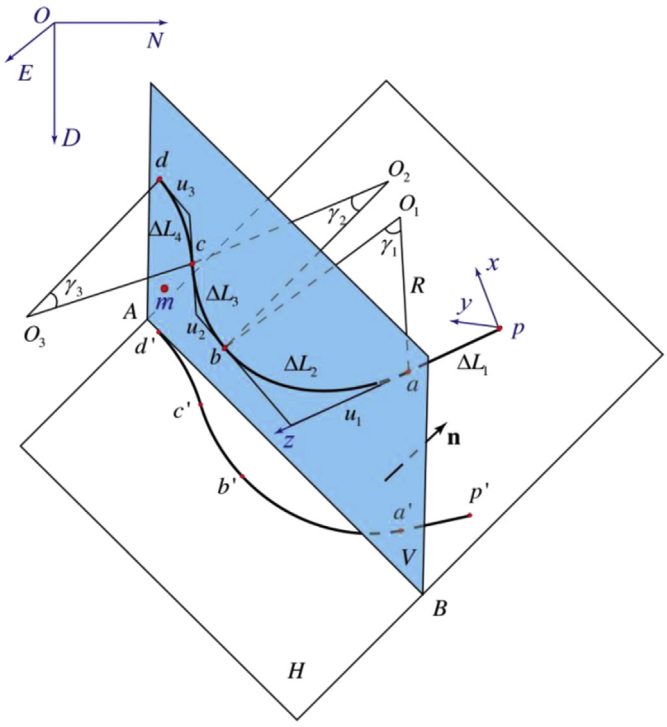

Fig. 10. Trajectory control model.

4.2. Control scheme

Known parameters: x_m, y_m and z_m, the Cartesian coordinate parameters of point m in the p–xyz converted from polar coordinate parameters measured by RMRS, m; $\Delta\varphi$, the difference value between the azimuths at point t and p, (°); α_p, the inclination of point p, (°); φ_p, the azimuth of point p, (°); R,radius of the arcs, m.

Constraints: the ending point is in plane V; the azimuth of the ending point parallels V.

Parameters to be calculated: ω_1, ω_2, ω_3, the initial high side tool face angles of arc ab, arc bc and arc cd, (°); ΔL_1, ΔL_2, ΔL_3, ΔL_4, the lengths of every section, m.

The trajectory control model shown in Fig. 10 was simplified to four cases according to the actual situation: whether $\Delta\varphi$ equals 0; whether the current borehole is approaching, departing from or parallel to the vertical plane V. Each case goes with a control model as shown in Fig. 11.

The four cases of the trajectory control model are given in Appendix A.

4.3. Case study

In the intersecting process between two horizontal wells, given $\alpha_p = 65°$, $\varphi_p = 50°$ and the build-up rate is 8°/30 m.When $\Delta\varphi = 10°$, the points m in the coordinate system p–xyz are $m_1(-10,5,55)$, $m_2(-10,5,45)$ and $m_3(-10,5,35)$. When $\Delta\varphi = 0°$, the point is $m_4(-10,2,35)$. Do trajectory design using method given above.

By calculation, the four measurement points mentioned above correspond to the four cases described in the former step.

(1) When $\Delta\varphi = 10°$ and $m_1(-10,5,55)$, which is the first case, $\Delta L_1 = 2.02$ m, $\Delta L_2 = 33.98$ m and $\omega_1 = 92.12°$. The trajectory parameters are displayed in Table 1.
(2) When $\Delta\varphi = 10°$ and $m_2(-10,5,45)$, which is the second case, $\Delta L_2 = 33.98$ m, $\Delta L_3 = \Delta L_4 = 16.43$ m, $\omega_1 = 92.12°$, $\omega_2 = 91.02°$ and $\omega_3 = 268.98°$. The trajectory parameters are displayed in Table 2.
(3) When $\Delta\varphi = 10°$ and $m_3(-10,5,35)$, which is the third case$\Delta L_2 = 33.98$ m, $\Delta L_3 = \Delta L_4 = 24.67$ m, $\omega_1 = 92.12°$, $\omega_2 = 91.54°$, $\omega_3 = 268.46°$. The trajectory parameters are displayed in Table 3.

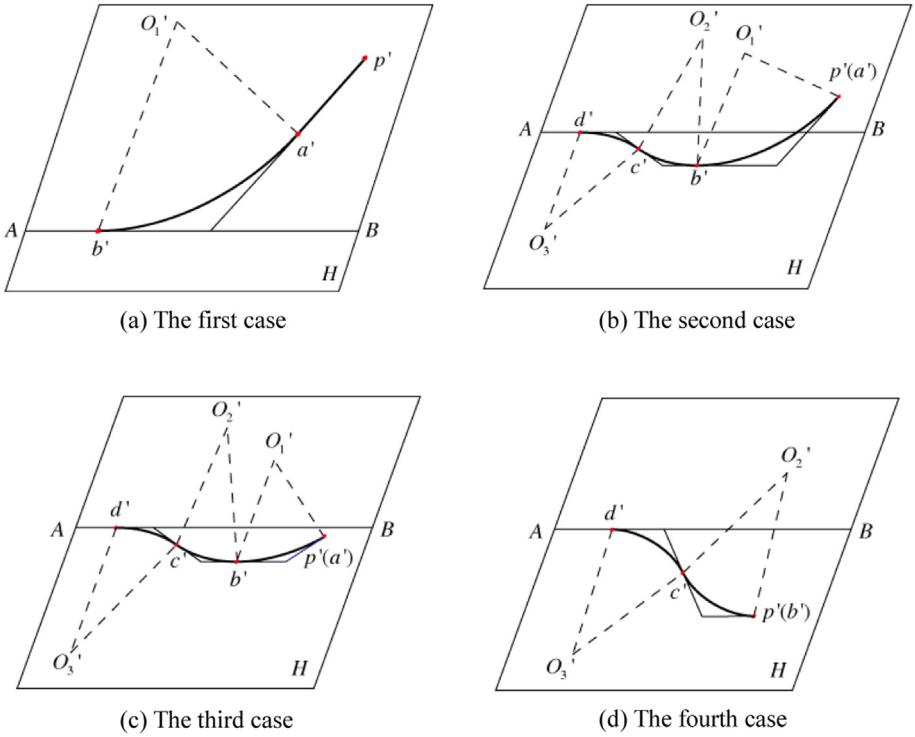

Fig. 11. Four cases from trajectory control model.

Table 1
Trajectory parameters when the azimuth difference is 10° and the point is m_1.

Section	MD/m	α/(°)	φ/(°)	N/m	E/m	TVD/m
Line *pa*	0.00	65.00	50.00	0.00	0.00	0.00
	2.02	65.00	50.00	1.18	1.41	0.86
Arc *ab*	12.02	64.93	52.94	6.82	8.49	5.09
	22.02	64.92	55.89	12.09	15.86	9.33
	32.02	64.97	58.83	16.98	23.48	13.56
	36.00	65.00	60.00	18.81	26.59	15.25

(4) When $\Delta\varphi = 0°$ and $m_4(-10,2,35)$, which is the fourth case, $\Delta L_3 = \Delta L_4 = 20.74$ m, $\omega_2 = 91.29°$, $\omega_3 = 268.71°$. The trajectory parameters are displayed in Table 4.

The coordinate parameters in the tables take the starting point of the profile as the origin for the sake of brevity.

It is obvious that the azimuth of the ending point d meets the demand. Next, the ending point will be confirmed to be whether in plane V or not.

The measure points in coordinate system O–NED are (25.49,38.16,32.31), (19.67,31.22,28.08), (13.84,24.28,23.85) and (16.14,22.35.23.85) while the ending points are (18.81,26.59,15.25), (31.42,51.56,28.28), (37.48,65.21,35.27) and (22.58,30.03,17.54). It is easy to confirm that the azimuth of the line determined by each two points from the first three groups is 60°, and that of the last group is 50°, which means that the ending points are in plane V. This proves the correctness of this trajectory control method.

5. Relative position error analysis

The relative position uncertainty analysis is still necessary in order to achieve accurate intersection, although the relative position error of RMRS does not accumulate but instead decreases gradually as drilling goes on.

5.1. Composition of relative position uncertainty

The intersecting process between two horizontal wells is a sequential guide process using RMRS. As shown in Fig. 5, the point m is the measure point, which passes through the point 1, 2, …, n; the point p is the bottom hole of the intersecting well, which passes through the point 1′, 2′, …, n'. Therefore, the relative position uncertainty between two horizontal wells during the intersecting process can be derived. As shown in Fig. 12, the position uncertainty of the intersection point t relative to the current bottom hole p consists of two parts: the position uncertainty of m relative to p and that of t relative to m.

The position uncertainty and the error ellipsoid (ellipse) which are used to reflect the size of the position uncertainty are presented in Appendix B.

Table 2
Trajectory parameters when the azimuth difference is 10° and the point is m2.

Section	MD/m	α/(°)	φ/(°)	N/m	E/m	TVD/m
Arc *ab*	0.00	65.00	50.00	0.00	0.00	0.00
	10.00	64.93	52.94	5.64	7.09	4.23
	20.00	64.92	55.89	10.91	14.45	8.47
	30.00	64.97	58.83	15.80	22.08	12.71
	33.98	65.00	60.00	17.63	25.18	14.39
Arc *bc*	43.98	64.98	62.94	21.96	33.14	18.62
	50.41	65.00	64.83	24.52	38.37	21.34
Arc *cd*	60.41	64.98	61.89	28.59	46.47	25.56
	66.83	65.00	60.00	31.42	51.56	28.28

Table 3
Trajectory parameters when the azimuth difference is 10° and the point is m3.

Section	MD/m	α/(°)	φ/(°)	N/m	E/m	TVD/m
Arc *ab*	0.00	65.00	50.00	0.00	0.00	0.00
	10.00	64.93	52.94	5.64	7.09	4.23
	20.00	64.92	55.89	10.91	14.45	8.47
	30.00	64.97	58.83	15.80	22.08	12.71
	33.98	65.00	60.00	17.63	25.18	14.39
Arc *bc*	43.98	64.96	62.94	21.96	33.14	18.62
	53.98	64.97	65.89	25.87	41.31	22.85
	58.65	65.00	67.26	27.56	45.20	24.83
Arc *cd*	68.65	64.96	64.32	31.27	53.46	29.06
	78.65	64.97	61.37	35.41	61.52	33.29
	83.32	65.00	60.00	37.48	65.21	35.27

Table 4
Trajectory parameters when the azimuth difference is 0° and the point is m4.

Section	MD/m	α/(°)	φ/(°)	N/m	E/m	TVD/m
Arc *bc*	0.00	65.00	50.00	0.00	0.00	0.00
	10.00	64.97	52.94	5.64	7.09	4.23
	20.00	65.00	55.89	10.92	14.46	8.46
	20.74	65.00	56.10	11.29	15.01	8.77
Arc *cd*	30.74	64.97	53.16	16.54	22.40	13.00
	40.74	65.00	50.22	22.15	29.51	17.23
	41.48	65.00	50.00	22.58	30.03	17.54

5.2. Case study

Given: $\alpha_p = 70°$; $\varphi_p = 270°$; $\alpha_t = 90°$; $\varphi_t = 90°$; $\Delta l = 30$ m; m(30,0,10), polar parameter of measure point in p-xyz; other parameters are displayed in Table 5 and Table 6.

Note: the borehole diameters of the two wells are 216 mm; the diameter of the stabilizer is 211 mm; the length between the bit and the stabilizer is 0.89 m; the length of the magnetic sub is 0.4 m; the length of the probe is 3 m. The following is obtained according to Eqs. (B.2) and (B.3): $\Delta C_4 = 0.111°$ and $\Delta C_5 = 0.095°$.

The following is relative position uncertainty analysis in the intersecting process between two horizontal wells.

(1) Determine the covariance matrix $\mathbf{COV_1}$

Convert polar coordinate (30,0,10) into Cartesian coordinate (10.4189,0,59.0885) according to Eq. (B.4).

Covariance matrix for precision errors of RMRS is obtained according to Eqs. (B.5), (B.6), (B.7) and (B.8):

$$\mathbf{H_1} = \begin{pmatrix} 0.3089 & -0.0003 & 0.1982 \\ -0.0003 & 0.0331 & 0 \\ 0.1982 & 0 & 1.4053 \end{pmatrix}$$

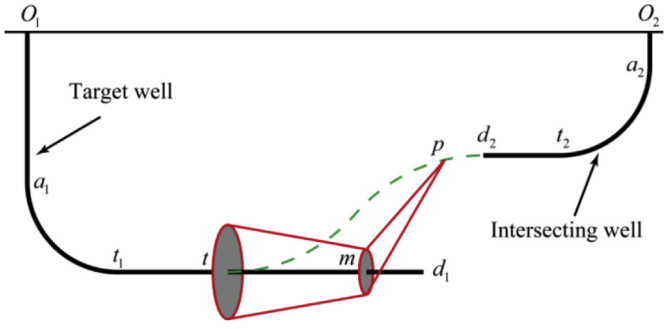

Fig. 12. Relative position uncertainty.

Table 5
The error of RMRS.

ΔC_1/(%)	ΔC_2/(°)	ΔC_3/(°)	ΔC_4/(°)	ΔC_5/(°)
2	1	0.5	0.111	0.095

Covariance matrix for misalignment error of magnetic sub is obtained according to Eq. (B.9):

$$\mathbf{H_2} = \begin{pmatrix} 0.0131 & 0 & -0.0023 \\ 0 & 0.0135 & 0 \\ -0.0023 & 0 & 0.0004 \end{pmatrix}$$

Covariance matrix for misalignment error of probe is obtained according to Eqs. (B.10), (B.11), (B.12) and (B.13):

$$\mathbf{H_3} = \begin{pmatrix} 0.0096 & 0 & -0.0017 \\ 0 & 0.0099 & 0 \\ -0.0017 & 0 & 0.0003 \end{pmatrix}$$

Covariance matrix for position uncertainty of m relative to p in Cartesian coordinate t-XYZ is obtained according to Eq. (B.14):

$$\mathbf{COV_1} = \begin{pmatrix} 0.3324 & 0.0003 & 0.1965 \\ 0.0003 & 0.0565 & -0.0001 \\ 0.1965 & -0.0001 & 1.4051 \end{pmatrix}$$

(2) Determine the covariance matrix $\mathbf{COV_2}$

Covariance matrix for position uncertainty of t relative to m in t-XYZ is obtained according to Eqs. (B.15) and (B.16):

$$\mathbf{COV_2} = \begin{pmatrix} 0.0713 & 0 & 0 \\ 0 & 0.6367 & 0 \\ 0 & 0 & 0.0009 \end{pmatrix}$$

(3) Determine the total covariance matrix **COV**

The total covariance matrix is obtained according to Eq. (B.17):

$$\mathbf{COV} = \begin{pmatrix} 0.4037 & 0.0003 & 0.1965 \\ 0.0003 & 0.6932 & -0.0001 \\ 0.1965 & -0.0001 & 1.4060 \end{pmatrix}$$

(4) Error ellipsoid and error ellipse

The eigenvalues of **COV** are: $\lambda_1 = 0.3666$, $\lambda_2 = 1.4432$ and $\lambda_3 = 0.6932$.

If the probability of relative position falling into the error ellipsoid is 95%, $k_1 = 2.796$. According to Eq. (B.19), the half-axes of the error ellipsoid are: $r_1 = 1.6928$ m, $r_2 = 3.3589$ m and $r_3 = 2.3279$ m.

According to Eqs. (B.20) and (B.21), the center of error ellipsoid in p-xyz is (20.6795,−0.1309,87.2792).

If the probability of relative position falling into the error ellipse is 95%, $k_2 = 2.448$. According to Eqs. (B.22), (B.23), (B.24) and (B.25), the half-axes of the error ellipse on the plane XY in t-XYZ are: $r_4 = 1.5554$ m and $r_5 = 2.0382$ m.

Table 6
The error of sophisticated magnetic inclinometer.

ΔC_{10}/(°)	ΔC_{20}/(°)	ΔC_{30}/(°)	ΔC_{40}/(°)	ΔC_{50}/(%)	ΔC_{60}/(°)
1.5	0.25	–	0.5	0.1	0.6

6. Conclusions

(1) The key issue restricting the intersection technology between two wells is that the intersection accuracy is not high. The development of control technique on navigating path can improve the accuracy for the intersection between two horizontal wells.

(2) Profile design of the intersection between two horizontal wells was given based on RMRS and uncertainty analysis. Both horizontal wells were designed double build-up profiles. The design was focused on intersection segment, extension segment, to-be-intersected segment and overlap segment, the analysis and parameter calculation of which determines the success or failure of the design. A larger build-up rate was recommended for the intersection segment in order to improve fault tolerance of the design; a reasonable vertical offset helps to reduce drilling costs; an accurate assessment of borehole position uncertainty improves the success rate of the intersection. The profile design reflects the integration of design and control, and has reference value for in-depth study and practice in the future.

(3) The existing methods on trajectory design with a given direction at target are not suitable for the intersection between two horizontal wells. The trajectory control model for intersecting process between two horizontal wells was established by using hold-inclination-and-adjust-azimuth pattern, which was based on an analogy between the intersection between two horizontal wells and the plane landing. The trajectory control model was simplified to four cases according to the actual situation, and a control scheme was given for each case. It was proven in the cases that the azimuth and position of the ending point obtained through the trajectory control method meets the expectation, which ensures the success rate of one-time intersection. Therefore, the control model applies to the intersection between two horizontal wells.

(4) The position uncertainty of the intersection point relative to the bottom of the intersecting well was calculated accurately based on RMRS and inclinometer. In this process, not only the error between measure point and bottom of intersecting well caused by RMRS, but also the error between intersection point and measure point caused by inclinometer working in the guide process of RMRS was taken into consideration. In addition, the error ellipsoid and error ellipse came from covariance matrix for relative position uncertainty have very important value in the intersection between two horizontal wells. The center of the error ellipsoid can be used as a target point for the correction trajectory design in the intersecting process between two horizontal wells, and the error ellipse can be used as the target window at the same time. Along with the drilling, the target point approaches the intersection point gradually, the target window narrows gradually, and finally an intersection between the two horizontal wells is realized.

Acknowledgments

The authors gratefully acknowledge the financial support from the National Natural Science Foundation of China (NSFC, 51221003, U1262201). This research is also supported by other projects (Grant numbers: 2013AA064803 , 2011ZX05009-005).

Appendix A. The four cases of the trajectory control model

The following preparations were done prior to elaboration on each case.

The unit normal vector $\mathbf{n}$ in *O–NED* is:

$$\mathbf{n} = \begin{bmatrix} \sin\ (\varphi_p + \Delta\varphi) \\ -\cos\ (\varphi_p + \Delta\varphi) \\ 0 \end{bmatrix} \tag{A.1}$$

The projected length D_p of vector $\mathbf{pm}$ on the unit normal vector $\mathbf{n}$ is:

$$D_p = |\mathbf{pm}\cdot\mathbf{n}| = \left| \mathbf{T_1} \begin{bmatrix} x_m \\ y_m \\ z_m \end{bmatrix} \cdot \begin{bmatrix} \sin\ (\varphi_p + \Delta\varphi) \\ -\cos\ (\varphi_p + \Delta\varphi) \\ 0 \end{bmatrix} \right| \tag{A.2}$$

where $\mathbf{T_1}$ is the transition matrix from *p–xyz* to *O–NED*:

$$\mathbf{T_1} = \begin{bmatrix} \cos\ \alpha_p \cos\varphi_p & -\sin\ \varphi_p & \sin\ \alpha_p \cos\ \varphi_p \\ \cos\ \alpha_p \sin\varphi_p & \cos\ \varphi_p & \sin\ \alpha_p \sin\ \varphi_p \\ -\sin\ \alpha_p & 0 & \cos\ \alpha_p \end{bmatrix} \tag{A.3}$$

Introducing a reference point $r(0,0,D_p/2)$ into coordinate system *p–xyz*, the projected length D_r of vector $\mathbf{rm}$ on the unit normal vector $\mathbf{n}$ is:

$$D_r = |\mathbf{rm}\cdot\mathbf{n}| = \left| \mathbf{T_1} \begin{bmatrix} x_m \\ y_m \\ z_m - D_p/2 \end{bmatrix} \cdot \begin{bmatrix} \sin\ (\varphi_p + \Delta\varphi) \\ -\cos\ (\varphi_p + \Delta\varphi) \\ 0 \end{bmatrix} \right| \tag{A.4}$$

The projected length D_1 of tangent length u_1 on the unit normal vector $\mathbf{n}$ is:

$$D_1 = \left| \mathbf{T_1} \begin{bmatrix} 0 \\ 0 \\ u_1 \end{bmatrix} \cdot \begin{bmatrix} \sin\ (\varphi_p + \Delta\varphi) \\ -\cos\ (\varphi_p + \Delta\varphi) \\ 0 \end{bmatrix} \right| = |u_1 \sin\alpha_p \sin\Delta\varphi| \tag{A.5}$$

where u_1 can be obtained by the following formula:

$$\gamma_1 = \arccos\left(\cos^2\alpha_p + \sin^2\alpha_p \cos\Delta\varphi\right),\ u_1 = R\tan\left(\gamma_1/2\right) \tag{A.6}$$

A.1. The first case

Conditions: $\Delta\varphi \neq 0$, $D_p \geq D_r$ and $D_p \geq D_1$.

In this case, the profile consists of two segments: line *pa* and arc *ab*. Horizontal projection of the profile on the plane H is shown in Fig. 11(a). The key parameters are:

$$\begin{aligned} \omega_1 &= \arccos\left(-\frac{\tan\ (\gamma_1/2)}{\tan\ \alpha_p}\right)\ \left(\Delta\varphi > 0\right), \\ \omega_1 &= 360 - \arccos\left(-\frac{\tan\ (\gamma_1/2)}{\tan\ \alpha_p}\right)\ \left(\Delta\varphi < 0\right)\ , \end{aligned} \tag{A.7}$$

$$\Delta L_1 = \left|\frac{D_p - D_1}{\sin\ \alpha_p \sin\Delta\varphi}\right|, \quad \Delta L_2 = \frac{\pi R\gamma_1}{180}. \tag{A.8}$$

A.2. The second case

Conditions: $\Delta\varphi \neq 0$, $D_p \geq D_r$ and $0 \leq D_p < D_1$.

In this case, the profile consists of three segments: arc *ab*, arc *bc* and arc *cd*. Horizontal projection of the profile on the plane H is shown in Fig. 11(b).

The following can be obtained from the geometric relationship and dogleg angle formula:

$$\begin{cases} \dfrac{(D_1 - D_p)/2}{\sin\ \alpha_p \sin\ \Delta\varphi'} = R\tan\ \left(\gamma_2/2\right) \\ \cos\ \gamma_2 = \cos^2\alpha_p + \sin^2\alpha_p \cos\ \Delta\varphi' \end{cases} \tag{A.9}$$

where $\Delta\varphi'$ is the azimuth adjustment of arc *bc* or *cd*, and $\gamma_2 = \gamma_3$.

In this case, the key parameters are:

$$\Delta L_2 = \frac{\pi R\gamma_1}{180}, \quad \Delta L_3 = \Delta L_4 = \frac{\pi R\gamma_2}{180} \tag{A.10}$$

when $\Delta\varphi > 0$,

$$\begin{aligned} \omega_1 &= \arccos\ \left(-\frac{\tan\ (\gamma_1/2)}{\tan\ \alpha_p}\right), \\ \omega_2 &= \arccos\ \left(-\frac{\tan\ (\gamma_2/2)}{\tan\ \alpha_p}\right), \\ \omega_3 &= 360 - \arccos\ \left(-\frac{\tan\ (\gamma_3/2)}{\tan\ \alpha_p}\right)\ ; \end{aligned} \tag{A.11}$$

When $\Delta\varphi < 0$,

$$\begin{aligned} \omega_1 &= 360 - \arccos\ \left(-\frac{\tan\ (\gamma_1/2)}{\tan\ \alpha_p}\right), \\ \omega_2 &= 360 - \arccos\ \left(-\frac{\tan\ (\gamma_2/2)}{\tan\ \alpha_p}\right), \\ \omega_3 &= \arccos\ \left(-\frac{\tan\ (\gamma_3/2)}{\tan\ \alpha_p}\right)\ . \end{aligned} \tag{A.12}$$

A.3. The third case

Conditions: $\Delta\varphi \neq 0$ and $D_p < D_r$.

In this case, the profile consists of three segments: arc *ab*, arc *bc* and arc *cd*. Horizontal projection of the profile on the plane H is shown in Fig. 11(c).

The following can be obtained from the geometric relationship and dogleg angle formula:

$$\begin{cases} \dfrac{(D_1 + D_p)/2}{\sin\ \alpha_p \sin\ \Delta\varphi'} = R\tan\ \left(\gamma_2/2\right) \\ \cos\ \gamma_2 = \cos^2\alpha_p + \sin^2\alpha_p \cos\ \Delta\varphi' \end{cases} \tag{A.13}$$

In this case, the calculation of key parameters is as same as that in the second case.

A.4. The fourth case

Conditions: $\Delta\varphi = 0$.

In this case, the profile consists of two segments: arc *bc* and arc *cd*. Horizontal projection of the profile on the plane H is shown in Fig. 11(d).

The following can be obtained from the geometric relationship and dogleg angle formula:

$$\begin{cases} \dfrac{D_p/2}{\sin\ \alpha_p \sin\ \Delta\varphi'} = R\tan\ \left(\gamma_2/2\right) \\ \cos\ \gamma_2 = \cos^2\alpha_p + \sin^2\alpha_p \cos\Delta\varphi' \end{cases} \tag{A.14}$$

In this case, the key parameters are:

$$\Delta L_3 = \Delta L_4 = \frac{\pi R\gamma_2}{180} \tag{A.15}$$

when $y_m \geq 0$,

$$\begin{aligned} \omega_2 &= \arccos\ \left(-\frac{\tan\ (\gamma_2/2)}{\tan\ \alpha_p}\right), \\ \omega_3 &= 360 - \arccos\ \left(-\frac{\tan\ (\gamma_3/2)}{\tan\ \alpha_p}\right)\ ; \end{aligned} \tag{A.16}$$

when $y_m < 0$,

$$\omega_2 = 360 - \arccos\left(-\frac{\tan(\gamma_2/2)}{\tan\alpha_p}\right),$$
$$\omega_3 = \arccos\left(-\frac{\tan(\gamma_3/2)}{\tan\alpha_p}\right). \quad \text{(A.17)}$$

Appendix B. The position uncertainty and the error ellipsoid (ellipse)

B.1. The position uncertainty of the measure point relative to the current bottom hole

The relative position measured by RMRS is independent from each other, and the relative position error, although present, is very small and not cumulative in successive measurements along with increase in measured depth. According to uncertainty model given by the industry steering committee for wellbore survey accuracy (ISCWSA) (Williamson, 1999, 2000), uncertainty of relative position measured by RMRS can be expressed as the following formula:

$$\mathbf{H} = \sum_{j=1}^{n} \mathbf{e_j} \mathbf{e_j}^{\mathrm{T}} \quad \text{(B.1)}$$

where, $\mathbf{H}$ is relative position uncertainty of all error sources combined at the measure point; $\mathbf{e_j}$ is measuring error vector caused by the number j independent error source at the measure point.

B.1.1. Error sources analysis

(1) Precision errors of RMRS

The part is error comes from imprecise manufacture and installation of RMRS, which is also influenced by the environment (like temperature) changes. Generally, the instrument is marked with error limits of relative distance, relative azimuth and relative tool face, respectively ΔC_1, %, ΔC_2, (°) and ΔC_3, (°), before shipped.

(2) Misalignment error of magnetic sub

Misalignment error of magnetic sub results from misalignment of the magnetic sub and the borehole axis, which is caused by the gap between borehole wall and stabilizers behind the magnetic sub.

Assume that outside diameter of the stabilizer is d_{S1}, m; diameter of the borehole is d_{H1}, m; the length between the bit and the stabilizer is l_1, m, then the misalignment error margin ΔC_4, (°) of magnetic sub can be expressed as:

$$\Delta C_4 = \arctan\left(\frac{d_{H1} - d_{S1}}{2l_1}\right) \quad \text{(B.2)}$$

(3) Misalignment error of probe

In order to ensure accuracy of the relative position, the probe needs to be tripped to appropriate depth of the first horizontal well with workover rigs and other tools. Misalignment error of probe is caused by bending and buckling of the tubing, top tensile force exerted by cable, bottom friction exerted by borehole and gravity of the probe itself.

Assume that outside diameter of the stabilizers installed above and below probe is d_{S2}, m; diameter of the borehole is d_{H2}, m; the length between the stabilizers is l_2, m, then the misalignment error margin ΔC_5, (°) of probe can be expressed as:

$$\Delta C_5 = \arctan\left(\frac{d_{H2} - d_{S2}}{l_2}\right) \quad \text{(B.3)}$$

B.1.2. Covariance matrix

As shown in Fig. 2, polar parameter $m(r,\theta_0,\varphi_0)$ detected by RMRS is converted into Cartesian coordinate parameter in the right-hand Cartesian coordinate system p-xyz as follows:

$$\begin{cases} x_m = r\sin\varphi_0\cos\theta_0 \\ y_m = r\sin\varphi_0\sin\theta_0 \\ z_m = r\cos\varphi_0 \end{cases} \quad \text{(B.4)}$$

which can be expressed as $\boldsymbol{r} = (x_m, y_m, z_m)^{\mathrm{T}}$.

(1) Covariance matrix for precision errors of RMRS

Measurement uncertainty of the relative distance:

$$\mathbf{e_1} = \Delta C_1 \boldsymbol{r} \quad \text{(B.5)}$$

Measurement uncertainty of the relative azimuth:

$$\mathbf{e_2} = \frac{\Delta C_2 \pi r}{180}\begin{pmatrix} \cos(\varphi_0 + \Delta C_2/2)\cos\theta_0 \\ \cos(\varphi_0 + \Delta C_2/2)\sin\theta_0 \\ -\sin(\varphi_0 + \Delta C_2/2) \end{pmatrix} \quad \text{(B.6)}$$

Measurement uncertainty of the relative tool face:

$$\mathbf{e_3} = \frac{\Delta C_3 \pi r \sin\varphi_0}{180}\begin{pmatrix} -\sin(\theta_0 + \Delta C_3/2) \\ \cos(\theta_0 + \Delta C_3/2) \\ 0 \end{pmatrix} \quad \text{(B.7)}$$

Therefore, the covariance matrix for precision errors of RMRS can be expressed as:

$$\mathbf{H_1} = \sum_{i=1}^{3} \mathbf{e_i} \mathbf{e_i}^{\mathrm{T}} \quad \text{(B.8)}$$

(2) Covariance matrix for misalignment error of magnetic sub

The relative position uncertainty caused by misalignment error of magnetic sub can be looked on as a disk with radius $\Delta C_4 \cdot r$ in the plane perpendicular to the borehole (Wolff and de Wardt, 1981). The contribution of this disk to the covariance matrix can be expressed as:

$$\mathbf{H_2} = \Delta C_2^4 \left[r^2 \begin{pmatrix} 1 & 0 & 0 \\ 0 & 1 & 0 \\ 0 & 0 & 1 \end{pmatrix} - \boldsymbol{r}\boldsymbol{r}^{\mathrm{T}} \right] \quad \text{(B.9)}$$

(3) Covariance matrix for misalignment error of probe

The probe is in the local coordinate system t-XYZ, and in order to get the covariance matrix, the relative position of p in t-XYZ is needed, which can be derived by introducing a coordinate transformation matrix.

The transformation matrix from t-XYZ to O–NED is:

$$\mathbf{T}_t = \begin{pmatrix} \cos\varphi_t & -\sin\varphi_t & 0 \\ \sin\varphi_t & \cos\varphi_t & 0 \\ 0 & 0 & 1 \end{pmatrix}\begin{pmatrix} \cos\alpha_t & 0 & \sin\alpha_t \\ 0 & 1 & 0 \\ -\sin\alpha_t & 0 & \cos\alpha_t \end{pmatrix} \quad \text{(B.10)}$$

where α_t and φ_t are inclination and azimuth of probe which can be measured by the probe itself.

The transformation matrix from *p-xyz* to *O–NED* is:

$$\mathbf{T}_p = \begin{pmatrix} \cos\ \varphi_p & -\sin\ \varphi_p & 0 \\ \sin\ \varphi_p & \cos\ \varphi_p & 0 \\ 0 & 0 & 1 \end{pmatrix} \begin{pmatrix} \cos\ \alpha_p & 0 & \sin\ \alpha_p \\ 0 & 1 & 0 \\ -\sin\ \alpha_p & 0 & \cos\ \alpha_p \end{pmatrix} \tag{B.11}$$

where α_p and φ_p are inclination and azimuth of magnetic sub which can be measured by the MWD.

Then, the relative position of *p* in *t-XYZ* is:

$$(X_p, Y_p, Z_p)^{\mathrm{T}} = -\mathbf{T}_t^{\mathrm{T}}\mathbf{T}_p(x_m, y_m, z_m)^{\mathrm{T}} \tag{B.12}$$

Therefore, covariance matrix for misalignment error of probe is:

$$\mathbf{H_3} = \Delta C_5^2 \left[r^2 \begin{pmatrix} 1 & 0 & 0 \\ 0 & 1 & 0 \\ 0 & 0 & 1 \end{pmatrix} - \begin{pmatrix} X_p \\ Y_p \\ Z_p \end{pmatrix} \begin{pmatrix} X_p, Y_p, Z_p \end{pmatrix} \right] \tag{B.13}$$

(4) Covariance matrix for position uncertainty of *m* relative to *p*

Since error sources are independent from each other, the covariance matrices can be added up directly. It is obvious that $\mathbf{H_1}$ and $\mathbf{H_2}$ are covariance matrices in p-xyz and $\mathbf{H_3}$ is in *t-XYZ*. So $\mathbf{H_1}$ and $\mathbf{H_2}$ are converted into *t-XYZ* by the transformation matrix for the sake of easy analysis and guidance of accurate intersection between two horizontal wells. The covariance matrix for position uncertainty of *m* relative to *p* in Cartesian coordinate *t-XYZ* is:

$$\mathbf{COV_1} = \mathbf{H_3} + \mathbf{T_t^T T_p}\left(\mathbf{H_1} + \mathbf{H_2}\right)\mathbf{T_p^T T}_t \tag{B.14}$$

B.2. The position uncertainty of the intersection point relative to the measure point

The borehole position uncertainty mainly comes from calculation error and instrument measurement error. Since the intersecting point and the measure point are at horizontal segment, the calculation error is negligible. Instrument measurement error consists of undefined systematic error and random error. The following is uncertainty analysis between two points using uncertainty model.

The covariance matrix for position uncertainty of *t* relative to *m* is:

$$\mathbf{H_4} = \begin{pmatrix} h_{11} & h_{12} & h_{13} \\ h_{21} & h_{22} & h_{23} \\ h_{31} & h_{32} & h_{33} \end{pmatrix} + \Delta C_{60}^2 \left[\Delta l^2 \begin{pmatrix} 1 & 0 & 0 \\ 0 & 1 & 0 \\ 0 & 0 & 1 \end{pmatrix} - \boldsymbol{a_5 a_5^{\mathrm{T}}} \right] \tag{B.15}$$

with

$$h_{11} = \sum_{j=1}^{5} \Delta C_{j0}^2 a_{j1}^2$$

$$h_{12} = h_{21} = \sum_{j=1}^{5} \Delta C_{j0}^2 a_{j1} a_{j2}$$

$$h_{13} = h_{31} = \sum_{j=1}^{5} \Delta C_{j0}^2 a_{j1} a_{j3}$$

$$h_{22} = \sum_{j=1}^{5} \Delta C_{j0}^2 a_{j2}^2$$

$$h_{23} = h_{32} = \sum_{j=1}^{5} \Delta C_{j0}^2 a_{j2} a_{j3}$$

$$h_{33} = \sum_{j=1}^{5} \Delta C_{j0}^2 a_{j3}^2$$

$$\boldsymbol{a_1} = \sin\ \alpha_t \cdot \Delta l \cdot (-\sin\ \varphi_t, \cos\ \varphi_t, 0)^{\mathrm{T}}$$

$$\boldsymbol{a_2} = \sin^2 \alpha_t \cdot \sin\ \varphi_t \cdot \Delta l \cdot (-\sin\ \varphi_t, \cos\ \varphi_t, 0)^{\mathrm{T}}$$

$$\boldsymbol{a_3} = \tan\ \alpha_t \cdot \Delta l \cdot (-\sin\ \varphi_t, \cos\ \varphi_t, 0)^{\mathrm{T}}$$

$$\boldsymbol{a_4} = \sin\ \alpha_t \cdot \Delta l \cdot (\cos\ \alpha_t \cos\ \varphi_t, \cos\ \alpha_t \sin\ \varphi_t, -\sin\ \alpha_t)^{\mathrm{T}}$$

$$\boldsymbol{a_5} = (\Delta N, \Delta E, \Delta D)^{\mathrm{T}}$$

where ΔC_{10} is compass reference error, (°); ΔC_{20} is drill string magnetization error, (°); ΔC_{30} is gyrocompass error, (°); ΔC_{40} is true inclination error, (°); ΔC_{50} is relative depth error, %; ΔC_{60} is misalignment error, (°); Δl is length of the borehole between measure point *m* and intersection point *t*, *m*.

Therefore, the covariance matrix for position uncertainty of *t* relative to *m* in Cartesian coordinate *t-XYZ* is:

$$\mathbf{COV_2} = \mathbf{T_t^T H_4 T_t} \tag{B.16}$$

B.3. Error ellipsoid and error ellipse

The total covariance matrix for position uncertainty of *t* relative to *p* in *t-XYZ* is:

$$\mathbf{COV} = \mathbf{COV_1} + \mathbf{COV_2} \tag{B.17}$$

COV can be rewritten as:

$$\mathbf{COV} = \begin{pmatrix} \mathrm{var}(X,X) & \mathrm{cov}(X,Y) & \mathrm{cov}(X,Z) \\ \mathrm{cov}(X,Y) & \mathrm{var}(Y,Y) & \mathrm{cov}(Y,Z) \\ \mathrm{cov}(X,Z) & \mathrm{cov}(Y,Z) & \mathrm{var}(Z,Z) \end{pmatrix} \tag{B.18}$$

(1) Error ellipsoid

Assume that λ_1, λ_2 and λ_3 are eigenvalues of **COV**, then:

$$r_1 = k_1\sqrt{\lambda_1},\ \ r_2 = k_1\sqrt{\lambda_2},\ \ r_3 = k_1\sqrt{\lambda_3} \tag{B.19}$$

where k_1 is the confidence factor; r_1, r_2 and r_3 are the half-axes of the error ellipsoid, *m*.

Because of the drill string magnetization, the center of the error ellipsoid O_3 deviates from the intersection point *t*. The vector $\mathbf{mO_3}$ in *O–NED* can be expressed as:

$$\mathbf{mO_3} = (\Delta C_{20} a_{21},\ \ \Delta C_{20} a_{22},\ \ 0)^{\mathrm{T}} - \boldsymbol{a_5} \tag{B.20}$$

The position of the center O_3 in the *p-xyz* can be expressed as:

$$\mathbf{pO_3} = \mathbf{T_p^T \cdot mO_3} + \boldsymbol{r} \tag{B.21}$$

(2) Error ellipse

The half-axes of the error ellipse on the plane *XY* in *t-XYZ* are:

$$r_4 = k_2\sqrt{\lambda_4},\quad r_5 = k_2\sqrt{\lambda_5} \tag{B.22}$$

where k_2 is the confidence factor; r_4 and r_5 are the half-axes of the error ellipse, m; λ_4 and λ_5 are the eigenvalues which can be obtained by the following equations.

$$\gamma = \frac{1}{2}\arctan\ \frac{2\mathrm{cov}(X,Y)}{\mathrm{var}(X,X) - \mathrm{var}(Y,Y)} \tag{B.23}$$

$$\lambda_4 = \mathrm{var}\left(X,X\right)\cos^2\gamma + \mathrm{var}\left(Y,Y\right)\sin^2\gamma + \mathrm{cov}\left(X,Y\right)\sin 2\gamma \tag{B.24}$$

$$\lambda_5 = \mathrm{var}\left(X,X\right)\sin^2\gamma + \mathrm{var}\left(Y,Y\right)\cos^2\gamma - \mathrm{cov}\left(X,Y\right)\sin 2\gamma \tag{B.25}$$

References

Al-Khodhori, S.M., Holweg, P., AlRiyami, H., 2008. Connector Conductor Wells Technology in Brunei Shell Petroleum-achieving High Profitability through Multiwell Bores and Downhole Connections. Paper presented at the IADC/SPE Drilling Conference, Orlando, Florida, USA, 4–6 March.

Cunnington, M., Hedger, L.K., 2010. Introduction of a New Well Design to the Narrabri Coal Seam Gas Project. Paper presented at the Asia Pacific Oil & Gas Conference and Exhibition, Brisbane, Queensland, Australia, 18–20 October.

Diao, B.B., Gao, D.L., Wu, Z.Y., 2012. Magnet ranging calculation method of twin parallel horizontal wells steerable drilling. J. China Univ. Pet. 35 (6), 71–75.

Gao, D.L., Guo, B.Y., Li, G.S., 2011. Optimized Design and Control Techniques for Drilling & Completion of Complex-structure Wells. China University of Petroleum Press, Dongying, pp. 1–14.

Ibatullin, R.R., Khisamov, R., Ibragimov, N.G., 2009. A Novel Thermal Technology of Formation Treatment Involves Bi-wellhead Horizontal Wells. Paper presented at the SPE Middle East Oil and Gas Show and Conference, Bahrain, Bahrain, 15–18 March.

Jia, Y.D., Wang, D.H., 2004. The technique of communicating DK-72B well with an old wellbore in Qatar. Pet. Drill. Tech. 32 (4), 82–83.

Kuckes, A.F., Hay, R.T., McMahon, J., Nord, A.G., Schilling, D.A., Morden, J., 1996. New electromagnetic surveying/ranging method for drilling parallel horizontal twin wells. SPE Drill. Complet. 11 (2), 85–90.

Lee, D., Brandao, F., 2005. U-tube Wells - Connecting Horizontal Wells End to End Case Study: Installation and Well Construction of the World's First U-tube Well. Paper presented at the SPE/IADC Drilling Conference, Amsterdam, Netherlands, 23–25 February.

Li, Z.F., Dai, J., 2008. Controlling technique on navigating path of horizontal butt well and crosswell. Nat. Gas. Ind. 28 (2), 70-72–167-168.

Liu, X.S., He, S.S., 2002. Well path soft landing design model and its application. Nat. Gas. Ind. 22 (2), 43–45+47.

Liu, S.B., Hong, F., Ling, J., 2005. Technology and application prospect of underground coal gasification. Nat. Gas. Ind. 25 (8), 119–122+117.

Mullin, S., Thorogood, J., Wright, J., Wardt, J.d., Bacon, R., 2013. Well Bore Collision Avoidance and Interceptions – State of the Art. Paper presented at the 2013 SPE/IADC Drilling Conference and Exhibition, Amsterdam, The Netherlands, 5–7, March.

Nie, M., Zhang, W., Lu, Z., Wang, C., Liu, Y., 2012. The Drilling Technique of the Parallel Horizontal Well of Steam-assisted Gravity Draingage and Vertical Well Connectivity. Paper presented at the IADC/SPE Asia Pacific Drilling Technology Conference and Exhibition, Tianjin, China, 9–11 July.

Oskarsen, R.T., Wright, J.W., Winter, D., Fitterer, D., Nekut, A.G., Sheckler, J.E., 2009. Rotating Magnetic Ranging Service and Single Wire Guidance Tool Facilitates in Efficient Downhole Well Connections. Paper presented at the SPE/IADC Drilling Conference and Exhibition, Amsterdam, The Netherlands, 17–19 March.

Peng, Z.Y., Xiao, J.G., Lu, X.W., 2009. Successful application of new technology of extracting brine from two horizontally diretional-communicated wells in xiangheng salt mine. China Well Rock Salt 40 (6), 19–22.

Poloni, R., Sassi, G., Valente, P., Campli, A.D., Bianchella, D., 2010. An Innovative Approach to Heat Heavy Oil Formations by Means of Two Horizontally Interconnected Wells. Paper presented at the SPE Annual Technical Conference and Exhibition, Florence, Italy, 19–22 September.

Shen, R., Qiao, L., Fu, L., Yang, H., Shi, W., 2012. Research and Application of Horizontal Drilling for CBM. Paper presented at the IADC/SPE Asia Pacific Drilling Technology Conference and Exhibition, Tianjin, China, 9–11 July.

Williamson, H.S., 1999. Accuracy Prediction for Directional MWD. Paper presented at the SPE Annual Technical Conference and Exhibition, Houston, Texas, 3–6 October.

Williamson, H.S., 2000. Accuracy prediction for directional measurement while drilling. SPE Drill. Complet. 15 (4), 221–233.

Wolff, C.J.M., de Wardt, J.P., 1981. Borehole position uncertainty – analysis of measuring methods and derivation of systematic error model. J. Pet. Technol. 33 (12), 2338–2350.

Zhang, Y., Zhang, G., Sun, F., Bao, Q., 2013. Application of U-shaped Wells Technologies for Efficient Stimulation of CBM. Paper presented at the 6th International Petroleum Technology Conference, Beijing, China, 26–28 March.